

# 11493

## A Study of Low-Reynolds Number Effects in Backward-Facing Step Flow Using Large Eddy Simulations

Lars Davidson\*

Dept. of Thermo and Fluid Dynamics  
Chalmers University of Technology  
S-412 96 Gothenburg, Sweden  
<http://www.tfd.chalmers.se/~lada>

Peter V. Nielsen

Dept. of Building Technology and Structural Engineering  
Aalborg University  
Sohngaardsholmsvej 57  
DK-9000 Aalborg, Denmark  
<http://www.civil.auc.dk/i6/staff/navn/i6pvn.html>

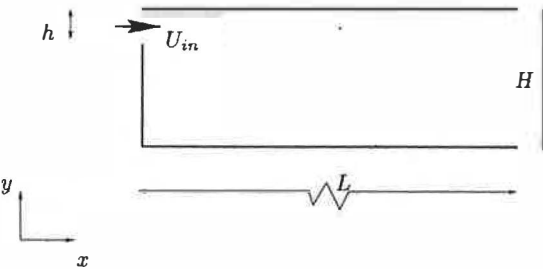


Figure 1: Configuration. Extent in  $z$  direction is  $0 \leq z \leq W$ .

### Abstract

The flow in ventilated rooms is often not fully turbulent, but in some regions the flow can be laminar. Problems have been encountered when simulating this type of flow using RANS (Reynolds Averaged Navier-Stokes) methods. Restivo [1] carried out experiment on the flow after a backward-facing step, with a large step (the ratio of the total height to the inlet is 6). This is much larger than what is common for backward-facing flow. The reason why Restivo chose this configuration is that it is similar to a ventilated room with the opposite wall removed. Detailed measurements were carried out in Ref. [1] at  $Re = 117$ ,  $780$  and  $Re = 5000$ . For the lowest Reynolds number the flow was fully laminar. At the intermediate Reynolds number the flow was partially, although not fully, turbulent. At the highest Reynolds number the flow was found to be fully turbulent. Thus we can identify three types of flows: laminar, transitional, and fully turbulent.

\*This work was carried out during the author's stay at Dept. of Building Technology and Structural Engineering, Aalborg University in Autumn 1997.

### Introduction

In the present study this flow will be computed using Large Eddy Simulations (LES). We have chosen the two Reynolds numbers investigated in Ref. [1] ( $Re = 780$  and  $5000$ ). Previously we have computed fully turbulent flow in a ventilated room using LES with good results [4]. A considerably more efficient numerical solver is used in the present study [5]. A dynamic one-equation model is used as a subgrid model [6].

Initially, we planned to also present simulations of the lowest Reynolds number  $Re = 117$  (i.e. laminar flow). However, it turned out that when the numerical predictions of the laminar flow were compared to the experiments of Restivo [1], we found a large discrepancy. This work is presented in Ref. [19]. We believe that there is something wrong in that experimental investigation. To support that conclusion, we present in Ref. [19] predictions of other backward facing flow configurations, where we show that our predictions agree well with experimental data.

In the following sections we present the subgrid model, the numerical method and results and discussions.

### The Dynamic One-Equation Subgrid Model

Recently a new dynamic one-equation subgrid model was presented [6]. For convenience, the model is briefly described below.

The modelled  $k_{sgs}$  equation can be written

$$\frac{\partial k_{sgs}}{\partial t} + \frac{\partial}{\partial x_j} (\bar{u}_j k_{sgs}) = \frac{\partial}{\partial x_j} \left( \langle C \rangle_{xyz} \Delta k_{sgs}^{\frac{1}{2}} \frac{\partial k_{sgs}}{\partial x_j} \right) + 2\nu_{sgs} \bar{S}_{ij} \bar{S}_{ij} - C_* \frac{k_{sgs}^{\frac{3}{2}}}{\Delta} \quad (1)$$

In the production term, the dynamic coefficient  $C$

$$P_{k_{sgs}} = -\tau_{ij}^a \bar{u}_{i,j}, \quad \bar{S}_{ij} = \frac{1}{2} \left( \frac{\partial \bar{u}_i}{\partial x_j} + \frac{\partial \bar{u}_j}{\partial x_i} \right) \quad (2)$$

$$\tau_{ij}^a = -2C \Delta k_{sgs}^{\frac{1}{2}} \bar{S}_{ij} = -2\nu_{sgs} \bar{S}_{ij}$$

is computed in a way similar to that used in the standard dynamic model [7, 8, 9, 10], i.e.

$$C = -\frac{\mathcal{L}_{ij} M_{ij}}{2M_{ij} M_{ij}}, \quad \mathcal{L}_{ij} = \widehat{\bar{u}_i \bar{u}_j} - \widehat{\bar{u}_i} \widehat{\bar{u}_j}$$

$$K = \widehat{k}_{sgs} + \frac{1}{2} \mathcal{L}_{ii}, \quad M_{ij} = \widehat{\Delta K^{\frac{1}{2}} \bar{S}_{ij}} - \Delta k_{sgs}^{\frac{1}{2}} \bar{S}_{ij} \quad (3)$$

where  $\mathcal{L}_{ij}$  denotes the *dynamic* Leonard stresses, and where  $K \equiv \frac{1}{2} \widehat{T_{ii}}$  is the subgrid kinetic energy on the test level [9, 10, 11].

To ensure numerical stability, a *constant* value of  $C$  in space ( $\langle C \rangle_{xyz}$ ) is used in the momentum equations. This is determined by requiring that the production in the whole computational domain should remain the same, i.e.

$$\langle 2C \Delta k_{sgs}^{\frac{1}{2}} \bar{S}_{ij} \bar{S}_{ij} \rangle_{xyz} = 2 \langle C \rangle_{xyz} \langle \Delta k_{sgs}^{\frac{1}{2}} \bar{S}_{ij} \bar{S}_{ij} \rangle_{xyz} \quad (4)$$

The idea is to include all local dynamic information through the source terms of the transport equation for  $k_{sgs}$ . This is probably physically more sound since large local variations in  $C$  appear only in the source term, and the effect of the large fluctuations in the dynamic coefficients will be smoothed out in a natural way. In this way, it turns out that the need to restrict or limit the dynamic coefficient is eliminated altogether.

## The Numerical Method

An implicit, two-step time-advancement methods is used [5]. The filtered Navier-Stokes equation for the  $\bar{u}_i$  velocity reads

$$\frac{\partial \bar{u}_i}{\partial t} + \frac{\partial}{\partial x_j} (\bar{u}_i \bar{u}_j) = -\frac{1}{\rho} \frac{\partial \bar{p}}{\partial x_i} + \nu \frac{\partial^2 \bar{u}_i}{\partial x_j \partial x_j} - \frac{\partial \tau_{ij}}{\partial x_j} \quad (5)$$

When it is discretized it can be written

$$\bar{u}_i^{n+1} = \bar{u}_i^n + \Delta t H (\bar{u}_i^n, \bar{u}_i^{n+1}) - \frac{1}{\rho} \alpha \Delta t \frac{\partial \bar{p}^{n+1}}{\partial x_i} - \frac{1}{\rho} (1 - \alpha) \Delta t \frac{\partial \bar{p}^n}{\partial x_i} \quad (6)$$

where  $H(\bar{u}_i^n, \bar{u}_i^{n+1})$  includes convection and the viscous and subgrid stresses, and  $\alpha = 0.5$  (Crank-Nicolson). Equation 6 is solved which gives  $\bar{u}_i^{n+1}$  which does not satisfy continuity. An intermediate velocity field is computed by subtracting the implicit part of the pressure gradient, i.e.

$$\bar{u}_i^* = \bar{u}_i^{n+1} + \frac{1}{\rho} \alpha \Delta t \frac{\partial \bar{p}^{n+1}}{\partial x_i} \quad (7)$$

Taking the divergence of Eq. 7 requiring that continuity (for the face velocities  $\bar{u}_{i,f}^*$  which are obtained by linear interpolation) should be satisfied on level  $n+1$  i.e.  $\partial \bar{u}_{i,f}^{n+1} / \partial x_i = 0$  we obtain

$$\frac{\partial^2 \bar{p}^{n+1}}{\partial x_i \partial x_i} = \frac{\rho}{\Delta t \alpha} \frac{\partial \bar{u}_{i,f}^*}{\partial x_i} \quad (8)$$

## Results

More detailed results are presented in Ref. [12].

The configuration is shown in Fig. 1. The geometry is given by:

$$W/H = 3, \quad h/H = 1/6, \quad Re = \frac{U_{in} h}{\nu}$$

Air of 20°C is used, and  $H = 3$  m. We use no-slip at all walls.  $y^+ < 2$  at the west wall, the floor and the ceiling; mostly it is below one. Near the side walls (low and high  $z$ )  $y^+$  is around 10. If  $y^+ > 11$ , wall functions are used [13]. The subgrid kinetic energy is set to zero at all walls as well as at the inlet. A convective boundary condition is used at the outlet for  $\bar{u}$ , i.e.

$$\frac{\partial \bar{u}}{\partial t} + U_b \frac{\partial \bar{u}}{\partial x} = 0.$$

where  $U_b$  is the bulk velocity ( $= U_{in} h / H$ ). This boundary condition has shown to be considerably better than zero streamwise gradient [14]. Zero streamwise gradient is used for  $\bar{v}$ .

A geometric stretching is used for the grid in the  $y$  direction, with refinement near the walls. The inlet is covered by 30 cells. In the  $x$  direction the cell spacing increases with  $x$ , and in the  $z$  direction a constant spacing is used; for more details see Table 1.

For the fully turbulent case ( $Re = 5000$ ) random fluctuation are superimposed on the experimental inlet velocity

$$\bar{u}_{in} = U_{in} + 2 \left( rnd - \frac{1}{2} \right) u'_{cxp}$$

$$\bar{v}_{in} = \left( rnd - \frac{1}{2} \right) u'_{cxp}, \quad \bar{w}_{in} = \left( rnd - \frac{1}{2} \right) u'_{cxp}$$

which gives a fluctuating amplitude  $u'_{cxp}$  (both positive and negative) for  $\bar{u}$ , and half of that for  $\bar{v}$  and  $\bar{w}$ . The inlet velocity  $U_{in}$  is constant over the inlet. In Ref. [12] another inlet boundary conditions is also presented where  $U_{in}$  is set according to experiments. As the inlet is rather small (large step height), the flow is probably less sensitive to the inlet boundary conditions than for configuration with a small step like that used in Ref. [15].

The time step is set to 0.26 seconds and 1.8 second for  $Re = 5000$  and  $Re = 780$ , respectively. This give a maximum convective CFL number of approximately one.

For  $Re = 5000$ , two different grids (one coarse and one fine) have been used. The number of cells in the  $x$  direction has been increased on the fine mesh. Unless otherwise stated, the results from the coarse mesh are presented below.

Mesh	$Re$	$\frac{\Delta x_{min}}{H}$	$\frac{\Delta x_{max}}{H}$	$\frac{\Delta y_{min,f}}{H}$	$\frac{\Delta y_{min,c}}{H}$	$\frac{\Delta y_{max}}{H}$	$\frac{\Delta z}{H}$	$L$
$160 \times 80 \times 64$	$Re = 780$	0.013	0.20	0.0016	0.043	0.04	0.047	$17.5H$
$128 \times 80 \times 80$	$Re = 5000$	0.013	0.17	0.0016	0.043	0.04	0.0375	$11.5H$
$128 \times 80 \times 128$	$Re = 5000$	0.013	0.17	0.0016	0.043	0.04	0.0234	$11.5H$

Table 1: Geometrical details of the meshes. The  $min$  denote the extent of the near-wall cell. Index  $c$  and  $f$  denote ceiling and floor, respectively.

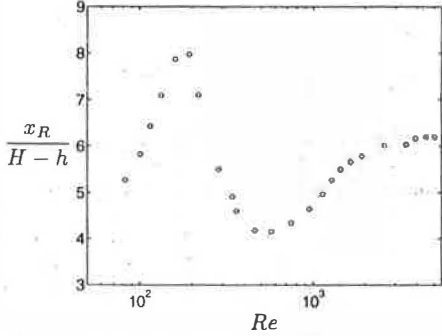


Figure 2: Experimental reattachment length  $x_R$  as a function of inlet Reynolds number  $Re$  [1].

The fine-mesh computations have been carried out on a 64 processor ORIGIN 2000 at Chalmers. The code was parallelized by Zacharov [16]. Using one/four/eight processors the elapsed time was 177/52/28 seconds per time step, thus giving a speed-up of 3.5 and 6.3 on four and eight processors, respectively.

The one-equation subgrid model presented above is used. The average value of the homogeneous constant in Eq. 4 is  $\langle C \rangle_{xyz} \approx 0.07$  for  $Re = 780$  and  $\langle C \rangle_{xyz} \approx 0.075$  for  $Re = 5000$ .

Vector plots are presented in Fig. 3. As can be seen the recirculation bubble is large for  $Re = 780$  ( $x_R/(H - h) = 9.2$ ). As a result the secondary bubble below the inlet is also large. The experimental data show the reverse: the recirculation region is larger for  $Re = 5000$  than for  $Re = 780$ , see Fig. 2. However, also the experiments show a larger bubble if the Reynolds number is reduced even further (down to  $Re \lesssim 250$ ). Other experimental investigations do not show such a marked dip in the  $x_R - Re$  curve as shown in Fig. 2. For example, neither the experimental investigation by Armaly *et al.* [17] nor by Romano *et al.* [18] present any similar dip. It should, however, be kept in mind that the step was smaller in these two investigations ( $h/H = .514$  and  $2/3$ , respectively). In a separate study, the present authors predict laminar flow in the Restivo-configuration [19]. It was concluded that for low  $Re$  numbers there are some problems with his measurements. Thus, considering the discrepancy between the predictions and experiments at  $Re = 780$ , we think that the predictions are more correct than are the experiments.

For  $Re = 5000$  the predicted reattachment length is  $x_R/(H - h) = 7.3$  and  $7.6$  for the coarse and fine mesh, respectively. This is some 20% larger than experimental data ( $x_{R,exp} = 6.12$ ). A number of fac-

tors can explain this discrepancy: too coarse a grid, inadequate subgrid model, inaccurate inlet boundary conditions, and, inaccurate measurements. Work is going on to investigate the influence of another inlet boundary conditions [12]. Two different grids have been used. As can be seen (Fig. 5) the difference between the predictions on the two grids is small except for  $x/h \geq 35$ . This is probably because the three-dimensional effects are large in the reattachment region (see Fig. 9), and these are convected downstream. If the velocity profiles are averaged over, for example,  $2H$  in the spanwise direction, the difference is much smaller [12]. It should be mentioned that the reattachment length has been accurately predicted with traditional low- $Re$  eddy-viscosity models such as the  $k - \epsilon$  model [2] and a modified  $k - \omega$  model [20].

In Figs. 4 and 5 the time-averaged  $\bar{u}$  velocities are compared with experiments. As mentioned above, we believe that the experimental data for  $Re = 780$  should be regarded with some caution.

No problems were experienced in performing the calculations for the low Reynolds number. The inlet boundary conditions are laminar, and a transition to turbulent flow occurs somewhere further downstream. In Fig. 6, the time history of the  $\bar{u}$  velocity at two points are shown which illustrates the transition. Close to the inlet ( $x/H = 5/6$ ), the fluctuating velocities are small whereas further downstream ( $x/H = 4$ ) they have grown much larger and the flow can be considered as turbulent. The rms-values  $u_{rms}/U_{in}$  at these two points (see Fig. 6) are 1.4% and 11.5%, respectively. The corresponding figures for  $Re = 5000$  are 4.6% and 13.8%, respectively [12]. Thus the growth of the fluctuations is much stronger for the low  $Re$  number case, in which the flow goes from laminar (the inlet), via transitional to fully turbulent. At the high  $Re$  number the flow is fully turbulent right from the inlet.

Attempts have been carried out to compute this flow at low Reynolds numbers by Skovgaard and Nielsen [2], where a low- $Re$  number  $k - \epsilon$  was used. No convergent results were obtained for  $Re < 1000$ . This is probably because as  $k$  goes towards zero, the  $\epsilon$  equation becomes ill-conditioned, because there are terms which include  $\epsilon/k$ . Peng *et al.* [3] used  $k - \omega$  models. The advantage of this type of model is that the  $\omega$  equations possesses a solution even if  $k \rightarrow 0$ . The production term and the turbulent diffusion terms go to zero, and the convection term, the destruction term and the viscous diffusion term balance each other. No convergence problems were reported. The same trend as in the present work was found, i.e. that the  $x_R$  increases when the  $Re$  number is reduced. In that work it was nevertheless concluded that the  $k - \omega$  failed, since the agreement with experimental data was very

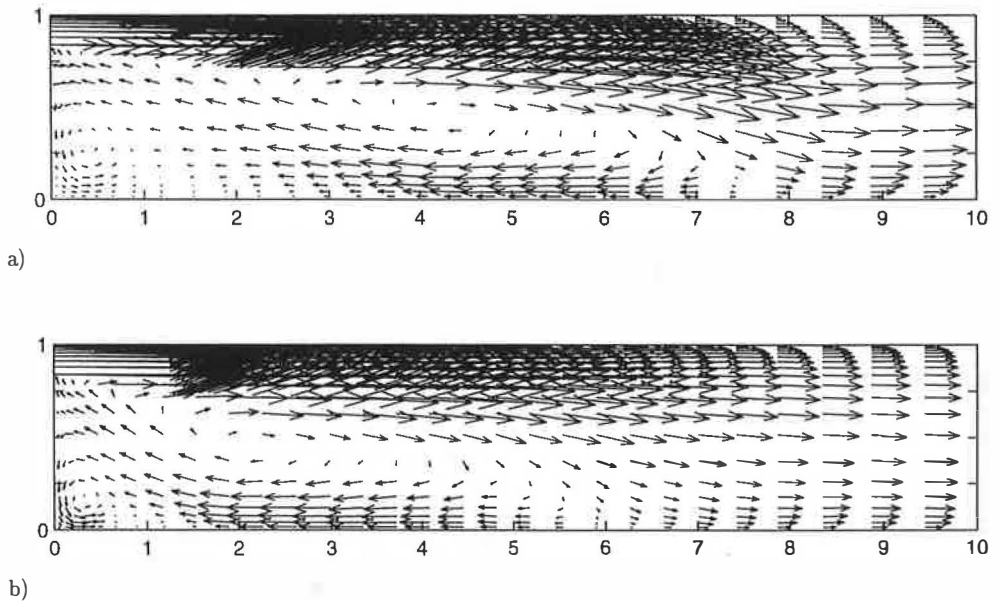


Figure 3: Time-averaged velocity vector plot (not to scale).  $z/W = 0.5$ . Every fourth vector is plotted in each direction. a)  $Re = 780$ . b)  $Re = 5000$ .

poor for low Reynolds numbers. In view of the findings in this work (including Ref. [19]), that conclusion was perhaps incorrect.

In Fig. 5, the velocities for the coarse mesh have been time averaged during 11000 (2860 seconds) and 17000 (4420 seconds), respectively. From Fig. 5 it seems that the time during which time averaging is performed is sufficient. The number of time steps for time averaging for the fine mesh is 18000; time averaging was performed for another 6000 time steps but the effect on the time averaged  $\bar{u}$  profiles was found to be negligible.

We can relate the time-averaging time to how long time  $T_{conv}$  it takes for a fluid to be convected past the recirculation region. This would correspond to a characteristic time unit. A “bulk” velocity for the flow past the recirculating region is  $U_{bulk} \simeq 0.5U_{in} = 0.5 \cdot 0.153 \simeq 0.076$  m/s. Thus, we get  $T_{conv} = x_R/U_{bulk} = 6 \cdot 3/0.076 = 237$  seconds. Thus the averaging time  $T_{aver}$  correspond to 12 and 18 characteristic time units, respectively. This should be compared to Aksevoll & Moin [21] and Yang & Ferziger [22] who used 50 and 3.8 corresponding characteristic time units, respectively. It should be remembered that they, in addition, performed spanwise averaging, as their flows were homogeneous in the spanwise direction. The time  $T_{aver}$  in the present work is similar to that used in Ref. [22], but considerably shorter than that used in Ref. [21]. In those studied, however, they also present correlations of resolved fluctuations, which usually require considerably longer averaging times.

In Fig. 7 the time history of the reattachment point  $x_R$  at the center plane is shown. It can be seen that  $x_R$  fluctuates much. No information on the time history

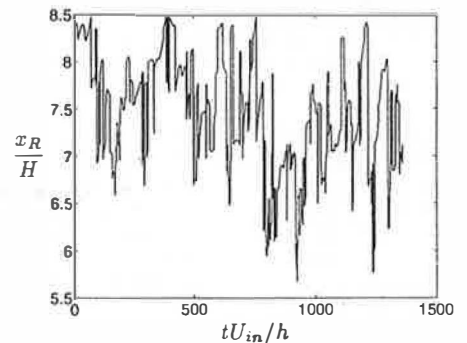


Figure 7: Time history of position of reattachment  $x_R$   $Re = 5000$ .  $z/W = 0.5$ .

for this  $Re$  number is provided in Ref. [1]. Romanc *et al.* [18] present time history of  $x_R$  in their configuration ( $h/H = 2/3$  and  $Re = 2500$ ), and they find that  $x_R/(H - h)$  oscillates between 2 and 10. In the DNS simulations of Le *et al.* [15] ( $h/H = 1/2$  and  $Re = 5000$ ) they find that  $x_R/(H - h)$  oscillates between 5 and 8.

In Figs. 8 and 9 the three-dimensionality of the flow field is illustrated. The contours of the  $\langle \bar{u} \rangle_t$  velocity contours close to zero are shown near the ceiling and near the floor (Fig. 8). We find that the main reattachment line is fairly straight for both  $Re$  numbers. There is larger spanwise variation for the secondary recirculation bubble below the inlet. The separation line for this bubble is  $x_R/H \simeq 3$  and 2 for  $Re = 780$  and  $Re = 5000$ , respectively. For the high Reynolds num

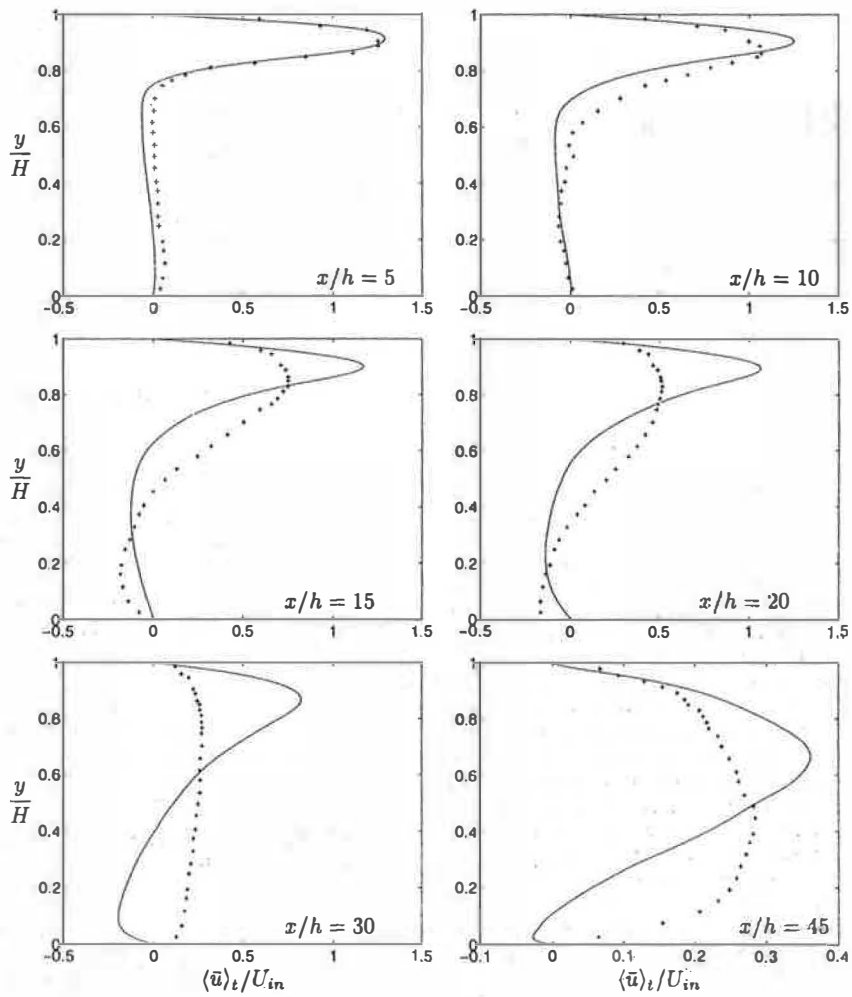


Figure 4: Time-averaged streamwise velocity  $\langle \bar{u} \rangle_t$ .  $Re = 780$ .  $z/W = 0.5$ . Lines: predictions; markers: experiments [1]

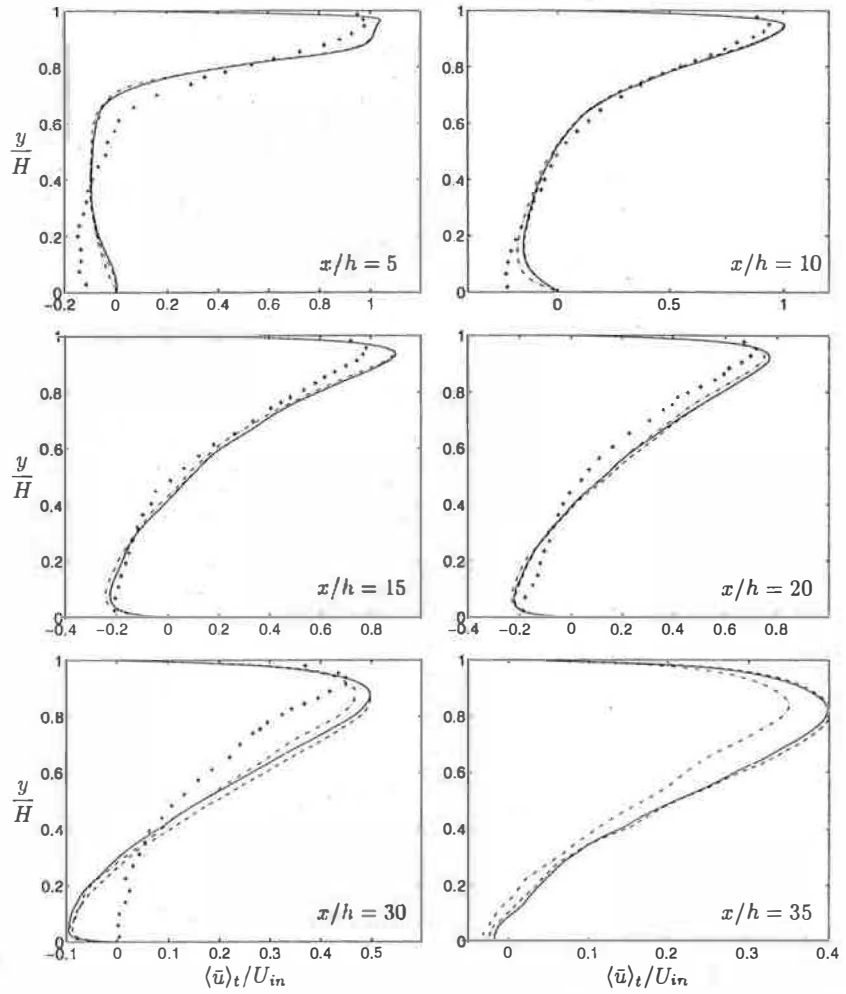


Figure 5: Time averaged streamwise velocity  $\langle \bar{u} \rangle_t$ .  $Re = 5000$ .  $z/W = 0.5$ . Solid lines: time averaged during 17 000 time steps ( $128 \times 80 \times 80$ ); dashed lines: time averaged during 11 000 time steps ( $128 \times 80 \times 80$ ); dash-dotted lines: time averaged during 18 000 time steps ( $128 \times 80 \times 128$ ); markers: experiments [1]

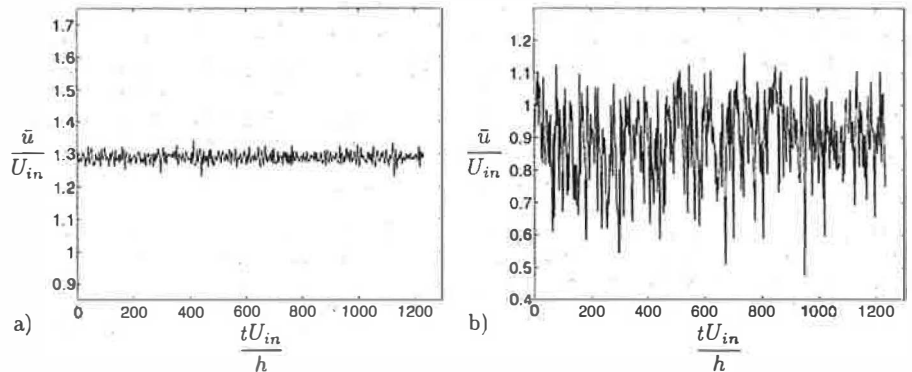


Figure 6: Time history of the  $\bar{u}$  velocity at two chosen points.  $z/W = 0.5$ .  $Re = 780$ . a)  $x/H = 5/6, y = 0.92H$   
b)  $x/H = 4, y = 0.92H$ .

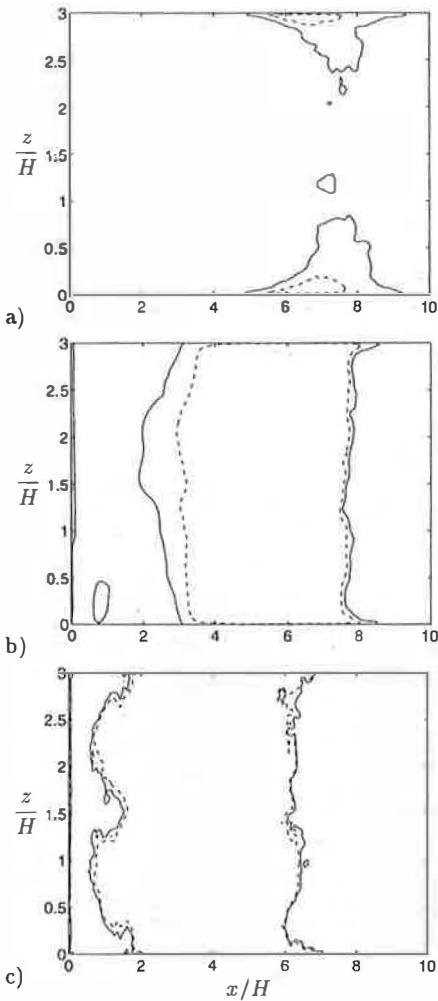


Figure 8: Contours of time averaged streamwise velocity  $\langle \bar{u} \rangle_t$  at the near-wall node. Solid line:  $\langle \bar{u} \rangle_t = 0$ ; dashed line:  $\langle \bar{u} \rangle_t / U_{in} = -0.002$ . a) Ceiling,  $Re = 780$ . b) Floor,  $Re = 780$ . c) Ceiling,  $Re = 5000$ .

ber there is no separation along the ceiling. However, for  $Re = 780$  we find separation along the side walls up to  $0.8H$  from the walls, see Fig. 8a. In the center plane, however, no separation takes place, which can also be seen from the vector field in Fig. 3. Note that we are here taking about *time averaged* flow field. *Instantaneously* there are negative  $\bar{u}$  velocities near the ceiling. The instantaneous recirculating regions are very thin, however.

In Fig. 9 time averaged  $\bar{u}$  profiles along spanwise lines are shown. It can be seen that the flow is not two-dimensional, but there are spanwise variations of up to approximately 10% of the inlet velocity.

## Conclusions

Large Eddy Simulations of the backwards-facing flow with a large step  $h/H = 1/6$ , have been presented for two different Reynolds number  $Re = 780$  and  $Re =$

5000.

Unfortunately, we believe that the experiments at this low-Re number should be regarded with some caution, because it has been found that the corresponding experimental investigation for laminar condition ( $Re = 117$ ) are likely to be incorrect [19].

For  $Re = 780$  the predictions show that the flow close to the inlet is close to laminar ( $u_{rms} \approx 0.01$ ), and that further downstream the flow becomes fully turbulent ( $u_{rms} \approx 0.11$ ). The predicted recirculation region is larger than for  $Re = 5000$ , an observation which has some support in the literature [17][18]. It has previously been found that the  $k - \epsilon$  model cannot handle this type of flow, and no convergent solutions are obtained [2]. The reason is that the  $\epsilon$  does not have any solution when  $k \rightarrow 0$ , because it includes terms like  $\epsilon/k$ . The  $k - \omega$  model, on the other hand, performs better, and convergent solutions are obtained [3]. Furthermore, the  $k - \omega$  model gives, as in the present work, an increasing  $x_R$  with decreasing  $Re$ .

At the high Reynolds number  $Re = 5000$  the agreement between predictions and experiments are fairly good, except in the reattachment region. The predicted recirculation region is some 20% larger than the experimental one. This discrepancy could be due to insufficient grid resolution, inadequate subgrid model, inadequate inlet boundary conditions, or inaccurate measurement data. Further investigations are needed, and some further work will be found in Ref. [12].

## References

- [1] A. Restivo. *Turbulent Flow in Ventilated Rooms*. PhD thesis, University of London, Imperial College of Science and Technology, Mechanical Engineering Department, 1979.
- [2] M. Skovgaard and P.V. Nielsen. Numerical investigation of transitional flow over a backward facing step using a low Reynolds number  $k - \epsilon$  model. In *12th AIVC-Conference on Air Movement Control within Buildings*, Ottawa, Canada, 1991.
- [3] S.-H. Peng, L. Davidson, and S. Holmberg. The two-equations turbulence  $k - \omega$  model applied to recirculating ventilation flows. Rept. 96/13, Dept. of Thermo and Fluid Dynamics, Chalmers University of Technology, Gothenburg, 1996.
- [4] L. Davidson and P. Nielsen. Large eddy simulations of the flow in a three-dimensional ventilated room. In S. Murakami, editor, *5th Int. Conf. on Air Distributions in Rooms, ROOMVENT'96*, volume 2, pages 161–168, Yokohama, Japan, 1996.<sup>1</sup>
- [5] L. Davidson. LES of recirculating flow without any homogeneous direction: A dynamic one-equation subgrid model. In *2nd Int. Symp. on Turbulence Heat and Mass Transfer*, pages 481–490, Delft, 1997. Delft University Press.<sup>1</sup>
- [6] L. Davidson. Large eddy simulation: A dynamic one-equation subgrid model for three-dimensional recirculating flow. In *11th Int. Symp. on Turbulent Shear Flow, Grenoble*, volume 3, pages 26.1–26.6, Grenoble, 1997.<sup>1</sup>

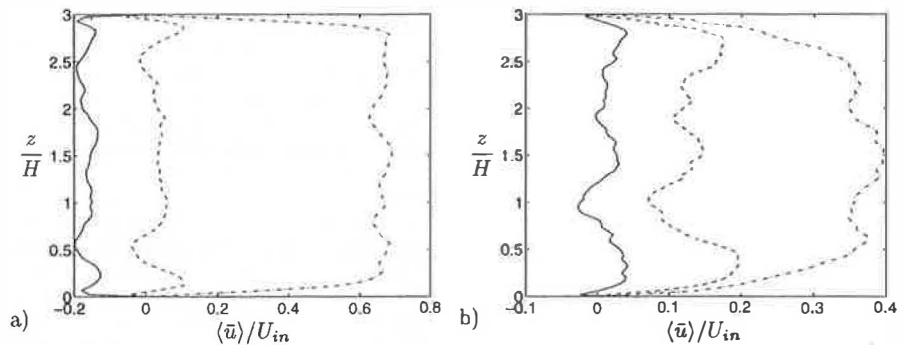


Figure 9: Time-averaged  $\bar{u}$  velocity.  $x/H = 6$ . Solid line:  $y/H = 0.16$ ; dashed line:  $y/H = 0.4$ ; dash-dotted line:  $y/H = 0.85$ . a)  $Re = 780$ . b)  $Re = 5000$ .

- [7] M. Germano, U. Piomelli, P. Moin, and W.H. Cabot. A dynamic subgrid-scale eddy viscosity model. *Physics of Fluids A*, 3:1760–1765, 1991.
- [8] M. Germano, U. Piomelli, P. Moin, and W.H. Cabot. Erratum. *Physics of Fluids A*, 3:3128, 1991.
- [9] S. Ghosal, T.S. Lund, P. Moin, and K. Akselvoll. A dynamic localization model for large-eddy simulation of turbulent flows. *Journal of Fluid Mechanics*, 286:229–255, 1995.
- [10] S. Ghosal, T.S. Lund, P. Moin, and K. Akselvoll. Corrigendum. *Journal of Fluid Mechanics*, 297:402, 1995.
- [11] L. Davidson. Large eddy simulations: A note on derivation of the equations for the subgrid turbulent kinetic energies. Rept. 97/11, Dept. of Thermo and Fluid Dynamics, Chalmers University of Technology, Gothenburg, 1997.<sup>1</sup>
- [12] L. Davidson and P.V. Nielsen. Low-Reynolds number effects in backward-facing step flow using large eddy simulations. Report, Dept. of Building Technology and Structural Engineering, Aalborg University, 1998.<sup>1</sup>
- [13] L. Davidson and B. Farhanieh. CALC-BFC: A finite-volume code employing collocated variable arrangement and cartesian velocity components for computation of fluid flow and heat transfer in complex three-dimensional geometries. Rept. 92/4, Dept. of Thermo and Fluid Dynamics, Chalmers University of Technology, Gothenburg, 1992.<sup>1</sup>
- [14] A. Sohankar, C. Norberg, and L. Davidson. Low-Reynolds number flow around a square cylinder at incidence: Study of blockage, onset of vortex shedding and outlet boundary condition. *Int. J. Num. Meth. Fluids*, 26:39–56, 1998.
- [15] H. Le, P. Moin, and J. Kim. Direct numerical simulation of turbulent flow over a backward-facing step. *Journal of Fluid Mechanics*, 330:349–374, 1997.
- [16] I. Zacharov. private communication. European Supercomputer Team, Silicon Graphics Inc., Switzerland, 1997.
- [17] B.F. Armaly, F. Durst, J.C.F. Pereira, and B. Schönung. Experimental and theoretical investigation of backward-facing step flow. *Journal of Fluid Mechanics*, 127:473–496, 1983.
- [18] G.P. Romano, S. Pomponio, and G. Querzoli. An investigation on the fluctuations of the reattachment point downstream backward facing step using particle tracking velocimetry. In *11th Int. Symp. on Turbulent Shear Flow, Grenoble*, volume 3, pages 30.7–30.12, 1997.
- [19] L. Davidson and P.V. Nielsen. A study of laminar backward-facing step flow. Report, Dept. of Building Technology and Structural Engineering, Aalborg University, 1998.<sup>1</sup>
- [20] S-H Peng, L. Davidson, and S. Holmberg. A modified Low-Reynolds-Number  $k - \omega$  model for recirculating flows. *ASME: Journal of Fluids Engineering*, 119:867–875, 1997.
- [21] K. Akselvoll and P. Moin. Large eddy simulation of turbulent confined coannular jets and turbulent flow over a backward facing step. Report no. TF-63, Stanford University, Dept. Mech. Eng., 1995.
- [22] K.-S. Yang and J.H. Ferziger. Large-eddy simulation of turbulent obstacle flow using a dynamic subgrid-scale model. *AIAA Journal*, 31:1406–1413, 1993.

<sup>1</sup>postscript file at <http://www.tfd.chalmers.se/~lada>